New Phytologist

Research

Tobacco leaf tissue rapidly detoxifies direct salt loads without activation of calcium and SOS signaling

Dorothea Graus[1]*, Kunkun Li[1]*, Jan M. Rathje[1], Meiqi Ding[1], Markus Krischke[2], Martin J. Müller[2], Tracey Ann Cuin[3], Khaled A. S. Al-Rasheid[4], Sönke Scherzer[1], Irene Marten[1], Kai R. Konrad[1] and Rainer Hedrich[1]

[1]Institute for Molecular Plant Physiology and Biophysics, University of Wuerzburg, Julius von-Sachs Platz 2, D-97082, Würzburg, Germany; [2]Institute for Pharmaceutical Biology, University of Wuerzburg, Julius von-Sachs Platz 2, D-97082, Würzburg, Germany; [3]Biological Sciences, School of Natural Sciences, University of Tasmania, Hobart Tas. 7005, Australia; [4]Zoology Department, College of Science, King Saud University, 11451, Riyadh, Saudi Arabia

Authors for correspondence:
Kai R. Konrad
Email: kai.konrad@botanik.uni-wuerzburg.de

Rainer Hedrich
Email: hedrich@botanik.uni-wuerzburg.de

Received: *11 February 2022*
Accepted: *11 September 2022*

New Phytologist (2023) **237:** 217–231
doi: 10.1111/nph.18501

Key words: calcium signaling, cytosolic pH, leaf response, NaCl transport, NHX1, osmotic effects, Salt Overly Sensitive pathway, salt stress.

Summary

- Salt stress is a major abiotic stress, responsible for declining agricultural productivity. Roots are regarded as hubs for salt detoxification, however, leaf salt concentrations may exceed those of roots. How mature leaves manage acute sodium chloride (NaCl) stress is mostly unknown.
- To analyze the mechanisms for NaCl redistribution in leaves, salt was infiltrated into intact tobacco leaves. It initiated pronounced osmotically-driven leaf movements. Leaf downward movement caused by hydro-passive turgor loss reached a maximum within 2 h.
- Salt-driven cellular water release was accompanied by a transient change in membrane depolarization but not an increase in cytosolic calcium ion (Ca^{2+}) level. Nonetheless, only half an hour later, the leaves had completely regained turgor. This recovery phase was characterized by an increase in mesophyll cell plasma membrane hydrogen ion (H^+) pumping, a salt uptake-dependent cytosolic alkalization, and a return of the apoplast osmolality to pre-stress levels. Although, transcript numbers of abscisic acid- and Salt Overly Sensitive pathway elements remained unchanged, salt adaptation depended on the vacuolar H^+/Na^+-exchanger NHX1.
- Altogether, tobacco leaves can detoxify sodium ions (Na^+) rapidly even under massive salt loads, based on pre-established posttranslational settings and NHX1 cation/H^+ antiport activity. Unlike roots, signaling and processing of salt stress in tobacco leaves does not depend on Ca^{2+} signaling.

Introduction

Salinity is a major threat to modern agriculture, causing decreased yields, the result of impaired crop growth. Plant responses to salinity can be divided into early membrane-associated fast processes related to osmotic and ionic stress and those regulated at the transcriptional level during the second phase (Läuchli & Grattan, 2007). The root is first to recognize major changes in soil salt concentration via monocation-induced calcium ion (Ca^{2+}) increase 1 (MOCA1; Jiang *et al.*, 2019), which within minutes, triggers a series of events comprising a rise in the cytoplasmic Ca^{2+} concentration ($[Ca^{2+}]_{cyt}$), membrane depolarization, massive release of potassium ions and increased Na^+/H^+-antiporter activity (Isayenkov & Maathuis, 2019). The root response to acute salt is associated with Ca^{2+} signals that travel to the shoot (Choi *et al.*, 2014; Xiong *et al.*, 2014). In turn, stomata close and cell expansion in the entire shoot ceases (Julkowska & Testerink, 2015). In roots, the salt stress response is regulated by the Salt Overly Sensitive (SOS) pathway (Ji *et al.*, 2013). This pathway includes the plasma membrane localized Na^+/H^+ antiporter SOS1 (NHX7), the SOS1-activating Ca^{2+}-dependent SOS2 (SnRK3.11/CIPK24)/SOS3(CBL4) module, the vacuolar cation/H^+ exchanger NHX1 and hydrogen ion (H^+) pumps at the plasma membrane and tonoplast (Liu & Zhu, 1998; Apse *et al.*, 1999; Halfter *et al.*, 2000; Palmgren, 2001; Qiu *et al.*, 2002). When plants face elevated salt concentrations for days or weeks, sodium ions (Na^+) and chloride ions (Cl^-) are transported to the shoot and far larger amounts of Na^+ accumulate in shoots compared to the roots (Baetz *et al.*, 2016; Darko *et al.*, 2017). In both root and shoot tissue, salt tolerance is enhanced by compartmentation of cytotoxic Na^+ and Cl^- loads into vacuoles by virtue of NHX- and CLC-type antiporters (Apse *et al.*, 1999; Subba *et al.*, 2021). To protect the cytosolic biochemistry from Na^+ and Cl^- entering the cell on its way to the vacuole, metabolic processes are remodeled to promote the production of compatible solutes such as proline and asparagine (Razavizadeh *et al.*, 2009; Patel *et al.*, 2020). A deeper reprogramming of gene expression occurs in plants growing at

*These authors contributed equally to this work.

extreme salt levels (Dinneny *et al.*, 2008; Wang *et al.*, 2016). Transcripts of rapid and transiently expressed genes are recognized already after 3 h, while bulk changes become visible after 24–72 h (Kreps *et al.*, 2002; Geng *et al.*, 2013; Baetz *et al.*, 2016).

Salt-tolerant signaling components identified in screens with Arabidopsis and potential candidates spotted in halophytes are often tested in tobacco to see if they play a protective role in defense against salt stress. This includes the vacuole localized NHX1 cation/H^+ antiporter, which when overexpressed, confers salt resistance to numerous crop species (Khan *et al.*, 2015; Wang *et al.*, 2018; Jegadeeson *et al.*, 2019; Guo *et al.*, 2020). To maintain the proton motive force for H^+-coupled transport, plasma membrane and vacuolar H^+-ATPases are activated by the SOS system and transcriptionally upregulated upon salt stress (Silva & Gerós, 2009; Gaxiola *et al.*, 2012; Małgorzata & Kabała, 2015). The pH gradient across the plasma and/or vacuole membrane are believed to drive Na^+/H^+ exchanger activity to limit the cytoplasmic Na^+ concentration (Yamaguchi *et al.*, 2005; Sze & Chanroj, 2018; Raddatz *et al.*, 2020).

Vacuolar pyrophosphatase (V-PPase, VHP) proton pump function becomes increasingly important under salt stress for generating the pH gradient necessary for proton-coupled Na^+ sequestration in leaves (Graus *et al.*, 2018). Salt induces the rise in V-PPase but not of V-ATPase pump currents (Graus *et al.*, 2018). Overexpression of the pyrophosphatase in leaves leads to higher vacuolar proton pump currents and vacuolar acidification. Hyper-acidification of the vacuole negatively feeds back to chloroplast photosynthesis and cell membrane potential. Overexpression of the pyrophosphatase from Arabidopsis or tobacco (AtVHP, NbVHP, respectively) causes the plasma membrane potential to drop in the absence but not in the presence of salt stress. This demonstrates that the VHP gene expression, thus V-PPase density and proton pumping, feedback on the plasma membrane electrical properties (Graus *et al.*, 2018).

Although vast progress has been made in the identification and unraveling of the molecular components involved in salt stress tolerance (Julkowska & Testerink, 2015), some aspects are still under debate (Britto & Kronzucker, 2015; Wu *et al.*, 2018; Isayenkov & Maathuis, 2019; Wu & Li, 2019). Questions about salt hardiness remain, particularly with regards to organ specific strategies. Salt sequestration in roots is thought to be mediated by Ca^{2+} signaling acting on the SOS pathway(s), but knowledge of the molecular mechanism for Na^+ and Cl^- sequestration in leaves remains fragmental.

Much of the knowledge about the mechanisms of salt tolerance in roots is based on relaxation analysis; i.e. by perturbing the cellular system, one can gain mechanistic insights into the responses at the cellular, molecular and macroscopic level. Roots can be directly challenged by specific sodium chloride (NaCl) doses, enabling in turn the study of the time-dependent responses. Such relaxation experiments with leaves are less straightforward and cannot be gained with plants watered with 200 mM NaCl via the soil. However, 3 d after such salt watering, the salt content in the leaves reaches a similar level to that obtained by direct infiltration of 200 mM NaCl into the apoplast of intact leaves (Graus *et al.*, 2018). Therefore, to carry out relaxation analysis with leaves comparable to roots, we took advantage of the infiltration approach for direct treatment of leaves. Monitoring the time-course of salt redistribution in salt-infiltrated leaves of intact tobacco plants, we studied the salt detoxification mechanisms in leaves. In response to the high salt load, leaves initially wilted, but turgor recovered rapidly after 2–3 h. Results obtained via a multidisciplinary approach provides unequivocal evidence that mature intact tobacco leaves are poised to overcome acute salt stress with well-established transporters operating independently of a cytoplasmic Ca^{2+} rise.

Materials and Methods

Plant materials and growth conditions

Nicotiana benthamiana Domin wild-type plants were cultivated on soil in a growth chamber for 4–6 wk with a day : night regime of 14 h : 10 h at 26°C : 22°C, a light intensity of 300 µmol m^{-2} s^{-1} and a humidity of *c.* 60%. Transgenic *Nicotiana tabacum* plants expressing CapHensor were sown in Murashige–Skoog-medium, 3% sucrose, 0.8% agar containing 25 mg ml^{-1} BASTA (DL-phosphinothricin), cultivated for 10–14 d and transferred to soil for a further 2–3 wk (see Li *et al.*, 2021). Transgenic *N. tabacum* plants expressing CapHensor were grown on the same growth medium and with the same conditions like the plants that were used for live-cell imaging on roots, but cultivated vertically for 7 d.

Leaf sample preparation and media

The procedure for epidermal strips and leaf disc preparation is described in detail in Li *et al.* (2021). The *N. benthamiana* leaf discs and transgenic *N. tabacum* epidermal strips were recovered in a standard solution for leaves (1 mM $CaCl_2$, 1 mM KCl and 10 mM MES, adjusted to pH 5.8 with bis-tris propane (BTP)). The *N. benthamiana* leaf discs were recovered overnight in darkness while the *N. tabacum* epidermal strips were recovered in white light for 3–6 h at room temperature.

Perfusion of the leaf discs or epidermal strips was performed with control solution (75 mM MES, 1 mM $CaCl_2$, pH 5.8 adjusted with Tris) that was isosmotic to the following standard solution additionally containing 50 mM NaCl adjusted with Tris to pH 5.8. Perfusion of guard cells was also performed with standard solution for leaves (1 mM $CaCl_2$, 1 mM KCl and 10 mM MES, adjusted to pH 5.8 with BTP) followed by the perfusion of a solution additionally containing 200 mM NaCl or 400 mM mannitol adjusted with BTP to pH 5.8, as indicated in the figure legends.

Salt infiltration of leaves

The entire leaf apoplast was infiltrated with different solutes through open stomata using 1 ml syringes. The infiltrated standard solution (control, agromix) normally used for agrobacteria-based transformation of *N. benthamiana* leaves (Jung *et al.*,

2015) consisted of 10 mM magnesium chloride ($MgCl_2$), 150 µM acetosyringone, 10 mM MES, pH 5.6/potassium hydroxide (KOH). The standard control/agromix solution was supplemented with either 50 mM NaCl, 100 mM NaCl, 200 mM NaCl, 200 mM potassium chloride (KCl), 200 mM sodium gluconate (Na-Gluc) or 400 mM sucrose. In the case of lanthanum administration, it was added to the control or 200 mM NaCl solution for a final concentration of 1 mM lanthanum(III) chloride ($LaCl_3$).

Imaging and quantification of leaf movement

To document the time course of leaf movement after solute infiltration (t_1), images were taken with a PowerShot A710IS camera (Canon, Tokyo, Japan) using the timelapse program gff. Later as a substitute, a Raspberry Pi® Camera Module V2 8MP color CMOS camera (Raspberry Pi® RPIZ CAM 6MM wide-angle objective) coupled to a Raspberry Pi 4, controlled via a Python script-driven by DEBIAN software was used to capture images over time. Images were used to determine the times (t_2, t_3) at which the infiltrated leaf had wilted and dropped to a maximum (t_2) and had subsequently fully recovered (t_3). The change in the leaf blade and petiole position between time t_1 and t_2 was calculated as a droop angle with the *angle tool* function of IMAGEJ v.1.51 (US National Institutes of Health; http://rsb.info.nih.gov/nih-image/). Violin plots were generated with OriginPro 2021 (OriginLab Corp., Northampton, MA, USA) and figures were arranged with CorelDraw 2018 (Corel Corp., Ottawa, ON, Canada).

Determination of apoplastic sodium content

Five leaves from different *N. benthamiana* plants were infiltrated with standard solution or salt-supplemented solution. After complete recovery of the plants from infiltration (2–5 h), leaves were detached, and their surface rinsed with distilled water. When the leaves were infiltrated a second time with distilled water, the leaf apoplast fluid was collected by centrifugation and the five samples obtained from each condition were combined to an appropriate volume as previously described (O'Leary *et al.*, 2014). Pooling of five infiltrated leaf samples from either standard or salt-supplemented solution infiltrated leaves represented one biological replicate each. This sample preparation procedure was repeated four times with different plant batches, resulting in four biological replicates for standard or salt-supplemented solution infiltrated leaves. The sodium content was measured with a flame photometer, Jenway PFP 7 (Jenway; http://www.jenway.com/).

Determination of proline and abscisic acid (ABA) content

Six leaves from different *N. benthamiana* plants infiltrated with 200 mM NaCl or control solution (10 mM $MgCl_2$, 10 mM MES, pH 5.6/KOH) were frozen (−80°C) and ground (six biological replicates). Subsequent extraction and chromatographic separation of plant material was carried out as described (Stingl *et al.*, 2013), using 5 ng of (D6)-ABA as internal standard. Abscisic acid content was analyzed by ultrahigh-performance liquid chromatography electrospray ionization tandem mass spectrometry (UHPLC-ESI–MS/MS) using a Waters Acquity I-Class UHPLC system (Milford, MA, USA) coupled to an AB Sciex 6500+ QTRAP® tandem mass spectrometer (AB Sciex, Framingham, MA, USA), operated in the negative ionization mode as previously described (Karimi *et al.*, 2021).

Proline content of tobacco leaves was measured according to the spectroscopic method described (Carillo & Gibon, 2011) and preparation of the samples was performed as mentioned earlier. Five biological replicates were used to quantify the proline content at the designated time points when leaves were infiltrated with standard solution or salt-supplemented solution. Briefly, 150 mg grinded freeze-dried samples were mixed in 40% ethanol and incubated at 4°C overnight. The supernatant was collected after centrifugation at 9600 ***g*** for 5 min. Then, 500 µl of the ethanol extraction or 100 µl standard solution were mixed with 1000 µl reaction mix (1% ninhydrin (w/v) in 60% acetic acid (v/v) and 20% ethanol (v/v)). After incubation at 95°C for 20 min and subsequent centrifugation for 1 min at 6700 ***g***, the samples (supernatant) absorption was measured at 520 nm with a spectrophotometer (lab/Hitachi U-1500; Hitachi, Tokyo, Japan). Proline concentration was determined according to the standard curve, and concentrations were calculated based on dry weight.

Quantitative real-time polymerase chain reaction

After solute infiltration, leaves were harvested at the times specified as t_1, t_2, t_3, immediately frozen in liquid nitrogen, crushed with a mortar and stored at −80°C until use. The total RNA was isolated with the Plant RNA Kit R6827-02 (OMEGA; www.omegabiotek.com). First-strand complementary DNA (cDNA) was then generated and used for quantitative real-time polymerase chain reaction (qRT-PCR) as described in Graus *et al.* (2018). The following primers were used for the qRT-PCR: NbVHP1fwd (5′-GTTGGA ATCTTGTTTGGC-3′) and NbVHP1rev (5′-GTAGGAGTG G TATTCGTT-3′), NbSOS1fwd (5′-TAGAAGAAGTCCGTGTC ACA-3′) and NbSOS1rev (5′-TCATCAACGGCTCAACCAC-3′), NbNHXfwd (5′-TTTTTCTGTGGGATCGT-3′) and NbN HXrev (5′-TTGAGCTAACCTGAACT-3′), NbACTfwd (5′-CC CAGAAGTCCTCTT-3′) and NbACTrev (5′-GGGATGCGAG GAT-3′), NbP5CS1fwd (5′-GAACGTGTTGGCACTCTGTT-3′) and NbP5CS1rev (5′-GTTAGCAAGCACACGGAAATAC-3′), NbP5CS2/4fwd: (5′-GCTGTAGGTGTTGGTCG TCA-3′) and NbP5CS2/4rev (5′-TAGTAGAGCTGCCAAACTGTC-3′), NbNCED3-1fwd (5′-CTGTTTCCACTTCAAAATCAACCAC-3′) and NbNCED3-1rev (5′-CGCCTTCA ACACATTTGGGT-3′), NbNCED3-2-fwd: (5′-GTACTATTTCCACTTCCACTTC-3′) and NbNCED3-2rev: (5′-ACGCCTTGAACGCATTCG-3′), NbABI1fwd (5′-GTACTGAGCCTGAC CTT-3′) and NbABI1rev (5′-AATGGACAACGGCATGGG-3′).

Chlorophyll fluorescence measurements

Chlorophyll fluorescence was determined with *N. benthamiana* plants dark-adapted for 30 min. Shortly before measurement, one

half of the selected leaf was infiltrated with control solution and the other half with control solution supplemented with 200 mM NaCl or KCl. Fluorescence acquisition and analysis were carried out with a Maxi PAM fluorometer (AVT 033) and the program IMAGING WIN v.2.41a FW Multi RGB (Walz, Effeltrich, Germany). To prevent the leaf blade coming out of focus, a fixed mesh was placed under the leaf. As a measure of photosynthetic stress, the quantum yield of light-induced nonphotochemical fluorescence quenching of photosystem II (Y(NPQ) = 1 − Y(II) − Y(NO) with Y(II) representing effective photochemical quantum yield of photosystem II and Y(NO) representing the quantum yield of nonlight induced nonphotochemical fluorescence quenching) was calculated from the minimum fluorescence of photosystem II (F_0) and the maximum fluorescence of dark-adapted cells (F_m) according to Kramer *et al.* (2004).

Membrane voltage recording *in planta*

Leaf discs of a 6 mm diameter mounted in a Petri dish lid with their adaxial side glued to double-sided adhesive tape and flooded with a control solution of 1.17 mM KCl, 1 mM $CaCl_2$, 9 mM $MgCl_2$, 10 mM MES, pH 5.6 were used to record voltage only. Samples were observed with an Axioskop 2FS microscope (Zeiss) using a water immersion objective (W Plan-Apochromat, 940/0.8; Zeiss) and illuminated with white light at an intensity of *c.* 150 µmol m^{-2} s^{-1} as described (Voss *et al.*, 2016). A piezo-driven micromanipulator (MM3A; Kleindiek Nanotechnik, Reutlingen, Germany) was used to impale the measuring electrode into the mesophyll cells near the edge of the leaf disc. The membrane potential was recorded with a custom-made headstage connected to a custom-made amplifier with an integrated differential amplifier (Ulliclamp-02) and the free software WINEDR (J. Dempster, University of Strathclyde, Glasgow, UK). After a stable free-running membrane voltage was recorded for at least 5 min, a NaCl (200 mM) containing solution was perfused at a rate of *c.* 4 ml min^{-1} for at least 5 min to completely replace the solution in the Petri dish lid. Synchronized fluorescence imaging and membrane potential recordings of *N. benthamiana* leaf discs expressing CapHensor was performed on an inverted microscope (AxioObserver; Zeiss) equipped with the appropriate fluorescence imaging hardware. The microscope setup and hardware for simultaneous electrophysiological and imaging recordings are described in detail in Gutermuth *et al.* (2013, 2018). Single-barreled microelectrodes were used with resistances between 60–120 MΩ. Control solution (75 mM MES, 1 mM $CaCl_2$, pH 5.8 adjusted with Tris) was isosmotic to the following solution additionally containing 50 mM NaCl adjusted with Tris to pH 5.8.

Imaging of CapHensor and GCaMP3

The imaging setup and analyzing software as well as the procedure of simultaneous wide-field Ca^{2+} and H^+ live-cell imaging in guard cells and mesophyll cells are described in detail in Li *et al.* (2021) and Gutermuth *et al.* (2013, 2018). The objectives used for guard cells and mesophyll cells were ×40 (C-Apochromat 40×/1.2 W Korr) and ×20 (Plan-Apochromat 20×/0.8), respectively. For Ca^{2+}-imaging in leave discs expressing GCaMP3, it was illuminated with 500 nm at an interval time of 5 s and an ET 535 ± 15 nm bandpass filter was used to capture the fluorescence under a ×10 objective (Plan-Apochromat 10×/0.45) covering a 0.8 cm × 0.8 cm field of view. Time-lapse fluorescence images were analyzed with the *multi measure* tool in the ROI manager module of IMAGEJ v.1.51 (National Institute of Health; http://rsb.info.nih.gov/nih-image/).

Confocal imaging of the tobacco roots was performed with a Leica TCS SP5 II equipped with a HCX IRAPO 25×/0.95 objective. Excitation of PRpHluorin and R-GECO1 was performed with an ultraviolet (UV) laser diode (405 nm), argon laser line 476 nm and a diode pumped solid state laser at 561 nm, respectively. PRpHluorin and R-GECO1 fluorescence was captured at 530 ± 30 nm and 617 ± 26 nm, respectively. Image processing was performed using FIJI/IMAGEJ v.1.50 or higher (National Institute of Health) and data were processed and plotted with IGOR PRO v.5.02 (Wavemetrics Inc., Portland, OR, USA).

Stomatal aperture measurements

Plants from the same sowing date were treated as follows. Two noninfiltrated plants were taken as controls (t_0), three were infiltrated with NaCl (200 mM) and three with agromix control solution. To determine the respective stomatal aperture, leaves were detached at the times t_0, t_1, t_2 and t_3 and immobilized with the abaxial side up onto double-sided adhesive tape. Using a water immersion objective (W Plan-Apochromat, 940/0.8; Zeiss), a CoolSNAP HQ camera (Visitron Systems, Puchheim, Germany) and the VISIVIEW Software (v.2.1.4; Visitron Systems), 20 images were taken for each condition at each time point. Image recording was accomplished within 5 min after leaf detachment. Such an experimental design was repeated seven times, with different plant batches. In a blind assay, the length and width of the stomatal pore from plants of seven different sowing dates were measured with IMAGEJ v.1.51 (National Institute of Health; http://rsb.info.nih.gov/nih-image/) and the ratio of pore width to length was determined. To quantify the dynamics of stomatal aperture over time from CapHensor-expressing guard cells in epidermal strips, the area within the pore was monitored using a custom-made macro in FIJI/IMAGEJ v.1.50 (Li *et al.*, 2021).

Scanning ion-selective electrode measurements

Ion-selective electrodes were fabricated from borosilicate glass capillaries (w/o filament, Ø 1.5 mm; Science Products GmbH, Hofheim, Germany) on a vertical puller (PC-10; Narishige, Tokyo, Japan). The tip of the capillaries was broken back to a size of *c.* 10 µm, then the capillaries were baked overnight at 220°C. The capillaries were then coated, at 220°C, with *N,N*-dimethyltrimethylsilylamine (Sigma-Aldrich) for 2 h. The H^+-selective electrodes were backfilled with 40 mM KH_2PO_4/15 mM NaCl, and the tip dipped in Hydrogen Ionophore I Cocktail A (Sigma-Aldrich). Potassium ion (K^+)-selective electrodes were backfilled with 200 mM KCl and tipfilled with the

Potassium Ionophore I Cocktail B (Sigma-Aldrich). Calibration of H^+-selective electrodes was performed at pH 4 and pH 7, and K^+-selective electrodes in solutions containing 10, 1 and 0.1 mM KCl. Only electrodes that recorded a shift in voltage of *c.* 58 mV per pH or pK unit were used. For dual H^+/K^+ flux recordings, the ion-selective electrodes were positioned *c.* 20 µm from the mesophyll tissue using the motion control system of Applicable Electronics in an upright microscope (Axioskop; Zeiss). The electrodes were connected via Ag/AgCl half-cells to the head stages (Applicable Electronics, Forestdale, MA, USA) of the microelectrode amplifiers. Electrodes were scanning at 10 s intervals over a distance of 100 µm, controlled by the custom made 'SISE-Monitor', a Labview-based program (National Instruments, Austin, TX, USA). Raw data were acquired with a NI USB 6259 interface (National Instruments) and these data were converted offline into ion flux data, with the SISE-Analyzer using the procedures as described (Arif *et al.*, 1995; Newman, 2001).

Results

Salt stress induces leaf movements

Leaves from *N. benthamiana* are a widely used model for testing gene function in salt stress (Yue *et al.*, 2012), particularly as they provide for an Agrobacteria infiltration-based transient transformation system (Goodin *et al.*, 2008). In leaves with open stomata, the Agrobacteria infiltrated moiety rapidly fills the substomatal cavities and intercellular air spaces entirely. In previous experiments, we have shown that *N. benthamiana* leaves transiently overexpressing V-PPases develop stress phenomena that leads to leaf necrosis, but not when a 200 mM NaCl load is provided alongside the transgene dose (Graus *et al.*, 2018). This behavior indicates that under conditions of a V-PPase 'overdose', a high salt load is beneficial. Here, we asked how nontransformed, mature leaves respond to the salt load alone. Application of 200 mM NaCl increased the osmolality of leaf apoplast by 425 mOsmol kg^{-1} (Graus *et al.*, 2018). Anticipating that a sudden strong rise in apoplast osmolality will drive water out of the mesophyll cells, we monitored leaf turgor via a video camera. The time course of leaf and petiole movement upon NaCl infiltration was compared to buffer controls (Fig. 1). Immediately after salt stimulus onset (at time t_1), leaf blades and petioles continuously lost turgor, while buffer control leaves did not (Fig. 1a). As a result of turgor loss, the salt infiltrated leaves and their petioles moved downward and at t_2 (within *c.* 116 min), reached maximal deflection of 40° and 14°, respectively (Video S1; Fig. 1a–c). While leave turgor loss was predicted, the fact that in the following *c.* 30 min (t_2–t_3) the leaves moved upwards again, finally reaching near pre-stimulus positions at t_3, was unexpected (Video S1; Fig. 1a–c). These movements indicate that leaf cells undergo a salt-induced turgor-loss-recovery cycle over a time of *c.* 150 min (Fig. 1c). Despite having a less pronounced wilting effect, a similar timing of the salt-induced turgor-loss-recovery cycle was apparent when lower salt loads such as 50 or 100 mM were used (Fig. S1). Thus, the salt transport capacity of the leaves is apparently not limited at 200 mM NaCl, a concentration where we can better follow the detoxification process at higher salt loads by stronger leaf movements (Fig. S1). When the leaf apoplast fluid was collected at t_3 and its Na^+ content was determined after 200 mM NaCl infiltration, the Na^+ load in the salt-stressed leaves was only 14 mM higher than in nonsalt-loaded leaves. This is only 8.3% of the infiltrated salt dose (Fig. 1d). However, 3–5 h after infiltration of the hyperosmotic NaCl solution, the total osmolality of the extracted leaf apoplast fluid was similar to control leaves, while the Na^+-content of the entire leaves remained high for days (Graus *et al.*, 2018). Thus, the infiltrated salt load did not remain in the leaf apoplast but was taken up and most likely sequestered in the cell vacuole (Conn & Gilliham, 2010).

Drop and recovery of photosynthesis mirrors salt detoxification kinetics

Photosynthesis is a proxy for a plant's ability to produce biomass, but it also represents a viability marker for toxic ion relations (James *et al.*, 2006). One would expect that toxic Na^+ quantities traveling through the cytoplasm to their vacuolar destination will not remain unrecognized by the chloroplasts (Stepien & Johnson, 2009). Hence, we followed the photosynthetic performance during leaf salt movement phases t_1–t_3. As representing the photosynthetic electron transport, we determined the quantum yield of light-induced nonphotochemical fluorescence quenching (Y(NPQ); Graus *et al.*, 2018) whereas a high Y (NPQ) correlates to a low photosynthetic rate. For better comparison and to limit variations between photosynthesis of different leaves, one half of the *N. benthamiana* leaves was loaded with control buffer and the other with the 200 mM NaCl buffer. Immediately after infiltration at t_1, Y(NPQ) in both leaf halves increased similarly: by 0.31 without NaCl and 0.32 with NaCl (Fig. S2a). This may indicate that photosynthesis initially suffers from reduced CO_2 partial pressure in the aqueous infiltrates. At t_2, Y(NPQ) of the control leaves recovered and maintained this low quenching level until t_3. The salt buffer-infiltrated samples had only partially recovered from nonphotochemical quenching at t_2, but at t_3 it was at the same level as the controls (Fig. S2a). This demonstrates that photosynthesis suppression accompanied leaf turgor loss at t_2 but had recovered by the time turgor was restored at t_3.

No restoration of pre-stress functional properties with membrane-impermeable salts

The initial response to a NaCl load is dominated by leaf cell dehydration. To understand the processes involved, we asked whether the leaf response is specific for NaCl or if the K^+ salt is similarly effective. When 200 mM NaCl was replaced by KCl, the resulting leaf movement did not significantly differ from the former (Fig. S3a–d). To our surprise, the KCl-induced increase and recovery of Y(NPQ) was the same as with the Na^+ salt (Fig. S2b). This indicates that osmotic water loss and suppression of photosynthesis is not Na^+ specific. Consequently, we assumed that the osmotic potential is what matters for the leaf cells. To

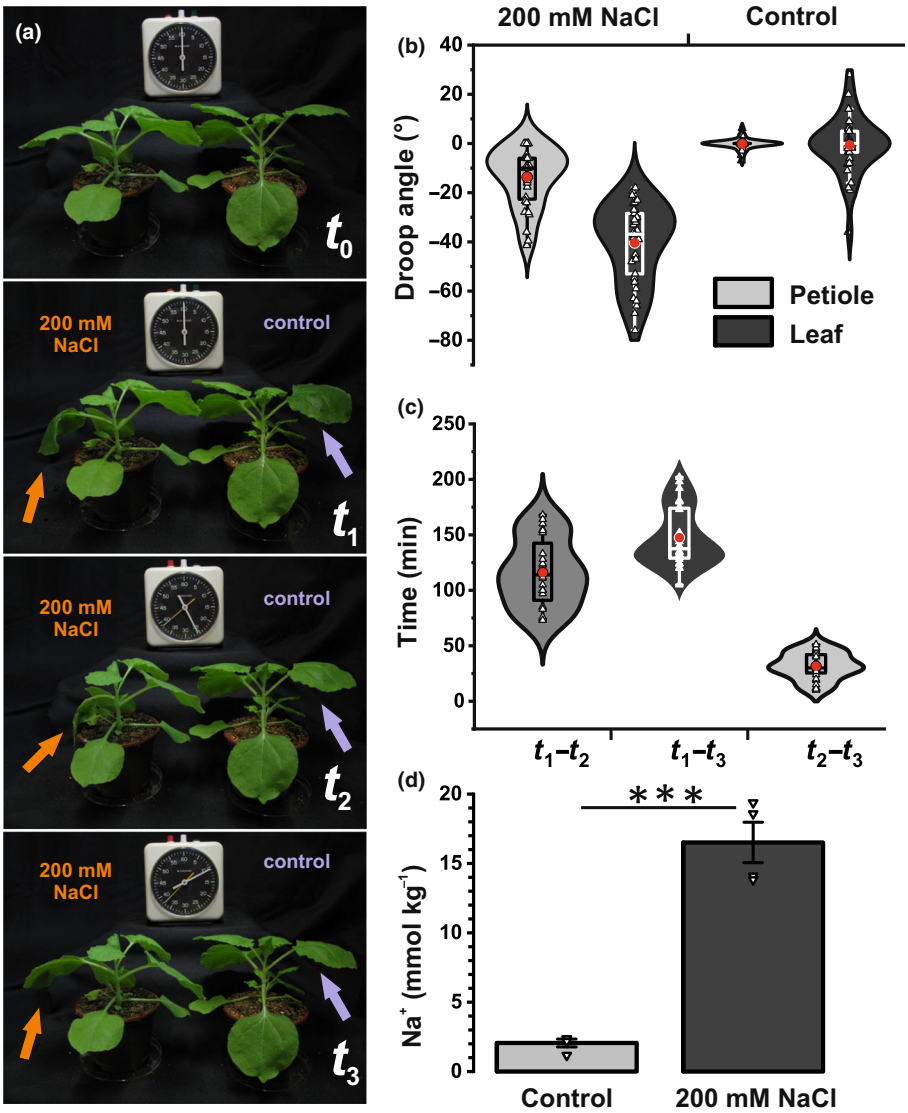

Fig. 1 Effect of high salt loads on *Nicotiana benthamiana* leaves. (a) Representative images of leaves before (t_0) and after infiltration of control (right) and 200 mM sodium chloride (NaCl)-containing solution (left) at different times. Images at time t_1 were taken immediately after infiltration and at later times, when the leaves had wilted and dropped to a maximum (t_2) or recovered from wilting completely (t_3). Infiltrated leaves are marked by an arrow. (b) Droop angle at t_2 measured separately for petiole and leaf blade under control and salt-loaded conditions. Data points represent means ± SE ($n = 36$–38). (b, c) Violin plot with integrated box plot diagram with median (black or white line in the square) and mean (red circle) values. Triangles represent individual data points. (c) Timespan between t_1–t_2, t_1–t_3 and t_2–t_3 ($n = 38$). (d) Apoplast sodium ion (Na^+) content at t_3 in control (light gray) and 200 mM NaCl (dark gray) infiltrated leaves. Data points represent means ± SE ($n = 4$). Asterisks indicate significant differences (***, $P < 0.001$, Student's *t*-test) between control and salt-treated leaves.

test this hypothesis, we replaced 200 mM NaCl with 400 mM sucrose. Indeed, when challenged with this sugar osmolyte, leaf movements were similar to the Na^+ and K^+ salt responses, although the time to reach t_2 and the time to recovery from wilting (t_2–t_3) almost doubled (Fig. S3e,f). This situation may be attributed to a weaker sugar than ion membrane transport capacity. A commonality of the chloride salts tested is that the plasma and vacuole membrane are permeable to Na^+, K^+, and Cl^-, and the corresponding ion channels and transporters have been identified and characterized to quite an extent (Assaha *et al.*, 2017; Wu, 2018). The same is true for the disaccharide sucrose and several monosaccharides (Chen *et al.*, 2015; Hedrich *et al.*, 2015; Raddatz *et al.*, 2020). What about a sodium salt with an anion that is membrane impermeable? In animal and plant electrophysiology, gluconate serves as a nonpermeant anion in combination with Na^+ and K^+. When we injected 200 mM Na-Gluc into the apoplast, leaf movement t_1–t_2 was like 200 mM NaCl, KCl, and 400 mM sucrose. However, in contrast to the other osmolytes, the turgor recovery phase was absent with Na-Gluc. Instead, the droop angle at t_3 remained at a level similar to that at t_2 (Fig. S3g). This behavior builds on the fact that (1) leaf movement t_1–t_2 is mainly based on osmotic water release from leaf cells and (2) turgor recovery during t_2–t_3 requires the uptake of the apoplast injected osmolytes Na^+ or K^+ and Cl^-.

Salt loads cause hydro-passive stomatal closure

We assume that wilting of the leaves after salt application can only recover to water potential levels before salt stress if the cell-apoplast continuum does not lose transpiration water to the environment. Since transpiration is controlled by guard cells, we studied stomatal apertures before (t_0) and after (t_1–t_3) 200 mM NaCl infiltration. Compared to noninfiltrated (t_0) and salt-free controls ($t_{1/2}$), the stomata of salt-treated leaves were closed at t_2 by 40–50% and did not re-open at t_3 (Fig. 2a). This shows that although ordinary leaf cells recover turgor in response to acute salt stress, the stomatal guard cells seem to reach pre-stress settings only after some delay. Thus, guard cells seem to handle acute salt stress differently to ordinary leaf cells.

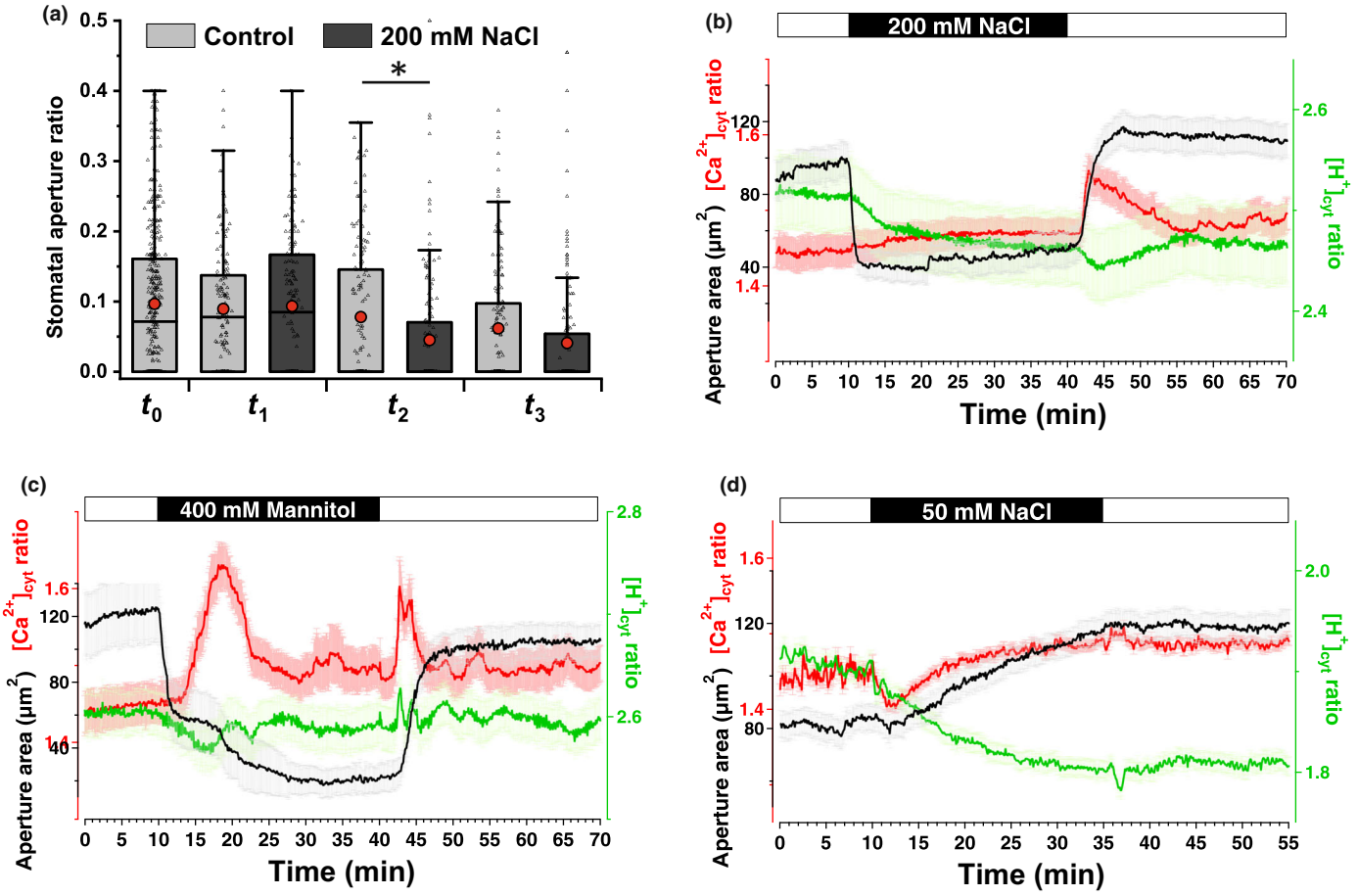

Fig. 2 Fast recovery of salt-loaded *Nicotiana benthamiana* leaves from wilting is calcium ion (Ca^{2+})- independent but associated with stomatal closure. (a) Box plot diagram with median (black line) and mean (red circle) values of stomatal aperture width : length ratios (mean ± SE, $n = 139–161$, for each treatment seven epidermal strips with *c*. 20 stomata each) determined from *N. benthamiana* leaves infiltrated with a control (gray bar) or 200 mM sodium chloride (NaCl; black bar) solution. Time point t_1 is immediately after infiltration, t_2 is at maximum leaf wilting and t_3 is the time point the leaves recovered from wilting. Note that the aperture ratio median values (black line) for control or salt solution treatment at t_2 and t_3 are congruent with the zero value. Significant differences are displayed by asterisks for selected conditions (*, $P < 0.05$, one-way ANOVA followed by Tukey's *post hoc* test). Triangles represent individual data points. (b–d) Simultaneous time-lapse imaging of $[Ca^{2+}]_{cyt}$- (red) and $[H^+]_{cyt}$-ratio (green) in guard cells during aperture monitoring (black) of *N. tabacum* stomata in epidermal strips stably expressing CapHensor. (b) Effect on $[Ca^{2+}]_{cyt}$, $[H^+]_{cyt}$ and aperture area during a shift from the standard solution (with low osmolality) to a 200 mM NaCl containing solution ($n = 24$). (c) Influence on $[Ca^{2+}]_{cyt}$, $[H^+]_{cyt}$ and aperture area by a 400 mM mannitol containing solution ($n = 18$), which is equivalent to the osmotic strength of the NaCl solution used in (b). Both, in (b) and (c), aperture area rapidly decreased in the presence of the highly osmolal NaCl or mannitol solution, which was fully reversible. While NaCl resulted in $[Ca^{2+}]_{cyt}$ elevations only upon wash-out, mannitol treatment results in a large $[Ca^{2+}]_{cyt}$ rise upon wash-in and a smaller $[Ca^{2+}]_{cyt}$ rise upon wash-out. Standard solution for leaves (1 mM $CaCl_2$, 1 mM KCl and 10 mM MES, adjusted to pH 5.8 with BTP) with or without addition 200 mM NaCl or 400 mM mannitol, adjusted with BTP to pH 5.8, was used. (d) Effect of salt treatment on $[Ca^{2+}]_{cyt}$, $[H^+]_{cyt}$ and aperture area when the perfused control solution (75 mM MES, 1 mM $CaCl_2$, pH 5.8 adjusted with Tris) was isosmotic to the NaCl (50 mM) solution ($n = 18$). A steady $[H^+]_{cyt}$-decrease (alkalization, as in (b)) and small transient $[Ca^{2+}]_{cyt}$ decrease is associated with stomatal opening in the presence of 50 mM NaCl. (b–d) Mean values over time are presented with SE values (light colored) from 18 to 24 biological replicates as indicated earlier.

Since hydro-active stomatal movement is known to be controlled by $[Ca^{2+}]_{cyt}$ and cytoplasmic H^+ concentrations ($[H^+]_{cyt}$), we monitored salt-induced changes using the dual Ca^{2+}/H^+-sensor CapHensor (Li *et al.*, 2021; Fig. 2b–d). When we perfused epidermal strips from *N. tabacum* leaves expressing the CapHensor with NaCl-free buffer, stomata remained open (Figs 2b, S4a). Following application of 200 mM NaCl, stomata closed within 1–2 min, and this was accompanied by an alkalization that reached a steady state after *c*. 5 min and lasted until the signal was terminated 30 min later (Figs 2b, S4a). In contrast, the $[Ca^{2+}]_{cyt}$ levels remained unchanged (Figs 2b, S4a) until stepping back to NaCl-free buffers. Under these conditions, stomatal apertures reached their pre-stimulus levels within 4–5 min (Figs 2b, S4a). A similar reversible stomatal movement was observed when 400 mM of the polyol osmolyte mannitol was administered instead of 200 mM NaCl (Figs 2c, S4b). This indicates that the guard cells' early salt response is hydro-passive (Raschke *et al.*, 1976) in nature. However, when the NaCl-free buffer was isoosmotic to the salt solution and the salt load was reduced to 50 mM NaCl, stomata opened further to reach a higher steady

state after *c.* 30 min (Figs 2d, S4c), indicating that guard cells power hydro-active stomatal opening using Na^+ and K^+ (Kronzucker *et al.*, 2013).

Turgor recovery does not involve changes in ABA and proline levels or SOS transcription

Both salt and drought stress are reported to lead to an adaptation of tissue osmolality governed by ABA signaling (Zhu, 2002; Yang & Guo, 2018). However, when we quantified the ABA content of the leaves at the different time-points (t_1–t_3) after injection with NaCl, the ABA levels were not considerably changed during the fast wilting-recovery cycle (Fig. 3a). Only at t_2 where the stomata of NaCl treated leaves where more closed than the control treated leaves (Fig. 2a), a significantly lower ABA level was apparent in the control leaves (Fig. 3a). The notion that salt-loaded leaves seem not to face severe dehydration is supported by our finding that production of the water stress osmolyte proline was not observed (Fig. 3b). In addition to ABA, sequestration of toxic Na^+ is regulated by the SOS signaling pathway. To address the question whether leaf recovery after salt infiltration is associated with transcriptional regulation of some SOS pathway components, we performed qRT-PCR analysis. The transcript levels in leaves of the Na^+ transporters NbSOS1 and NbNHX1, as well as NbVHP1 were not changed in response to salt loads at any time point $t_{1/2/3}$ (Fig. 4a–c). In addition, transcripts of the key genes of ABA biosynthesis (NCED3.1, NCED3.2) and highly ABA-responsive signaling component NbABI1 were not significantly altered (Figs 4d, S5a,b). The level of messenger RNAs (mRNAs) of P5CS1 and P5CS2–4 coding for enzymes with key functions in the production of the compatible solute proline also remained unchanged (Fig. S5c,d). Thus, neither transcriptional upregulation nor ABA or compatible solute proline synthesis is required to overcome salt-induced leaf wilting. In contrast, pre-established transport mechanisms are poised to clear the apoplast and cytoplasm of unfavorable Na^+/K^+ and Cl^- moieties during acute salt stress.

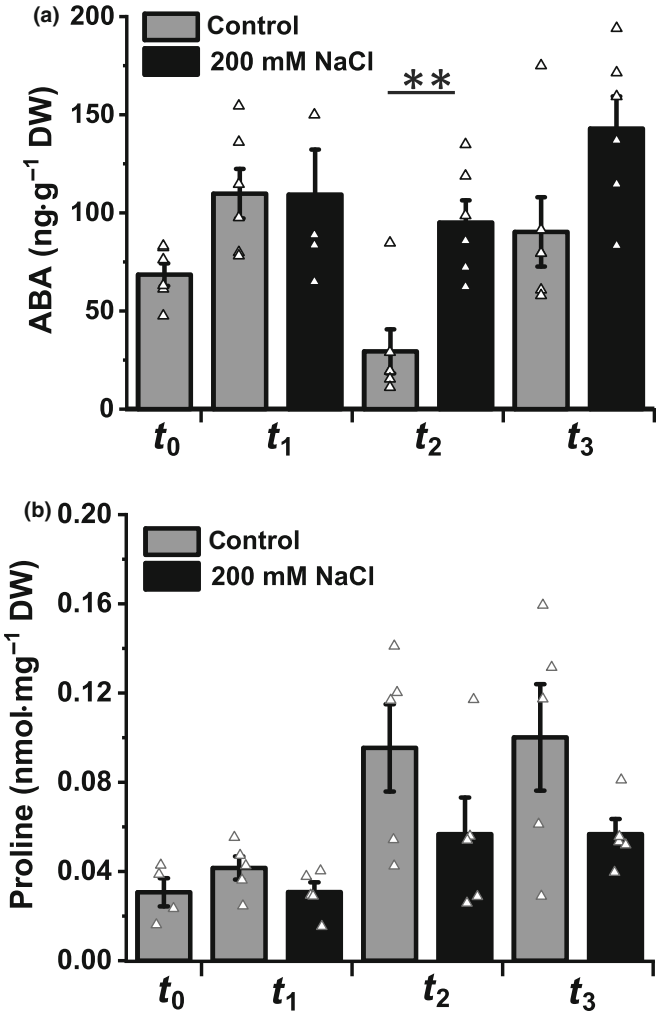

Fig. 3 Recovery of salt-loaded *Nicotiana benthamiana* leaves from wilting is independent of abscisic acid (ABA) and proline synthesis. Quantification of ABA (a) and proline (b) content from leaves at times t_1, t_2 and t_3 after the leaves were loaded with control (gray bar) or 200 mM sodium chloride (NaCl; black bar) solution. Time point t_1 is immediately after infiltration, t_2 is at maximum leaf wilting and t_3 is the time point the leaves recovered from wilting. In (a, b), the number of experiments were $n = 6$ and $n = 5$ (means ± SE), respectively. DW, dry weight. Triangles represent individual data points from biological replicates. Asterisks indicate significant differences (**$P < 0.01$, two-way ANOVA followed by Tukey's *post hoc* test) between control and salt-treated leaves.

Salt load processing is under the control of the electrochemical potential but not of Ca^{2+} signaling

Cellular import of Na^+ depends on both a positively charged gradient for this alkali metal ion and a negative membrane potential. In contrast to Na^+, the negatively charged Cl^- moiety is repelled by the negative electric field across the plasma membrane. Thus, to pass the plasma membrane barrier, anions must be co-transported with cations, most likely protons by using the proton motive force, to ensure electro-neutrality (Hedrich, 2012; Li *et al.*, 2017). Consequently, the important transport of both ions (Fig. S3) depends and feeds back on the membrane potential. We thus recorded the free-running membrane potential of mesophyll cells during sudden salt exposure. For this, voltage-recording microelectrodes were inserted into mesophyll cells located at the rim of a leaf disc, and the membrane potential was monitored in response to perfusion with a 200 mM NaCl buffer for *c.* 10 min. Upon salt exposure, the membrane potential depolarized by about *c.* 40 mV within about 7 min from an average resting state of −146 mV ($n = 21$; Fig. 5a). The membrane voltage did recover to pre-stimulus levels within *c.* 60 min when the 200 mM NaCl was replaced by a salt-free buffer (Fig. 5a), but remained depolarized when the salt load was present throughout (Fig. S6).

Recently, we have shown that mesophyll depolarization is accompanied by a pronounced activation of the voltage-dependent plasma membrane H^+-pump to counteract a depolarized plasma membrane (Reyer *et al.*, 2020; Zhou *et al.*, 2021a). In experiments with noninvasive ion-selective electrodes, we addressed whether extracellular H^+ activities change during the salt-induced depolarization phase of leaf cells. The use of extracellular ion-selective electrodes is ideal for monitoring ion fluxes

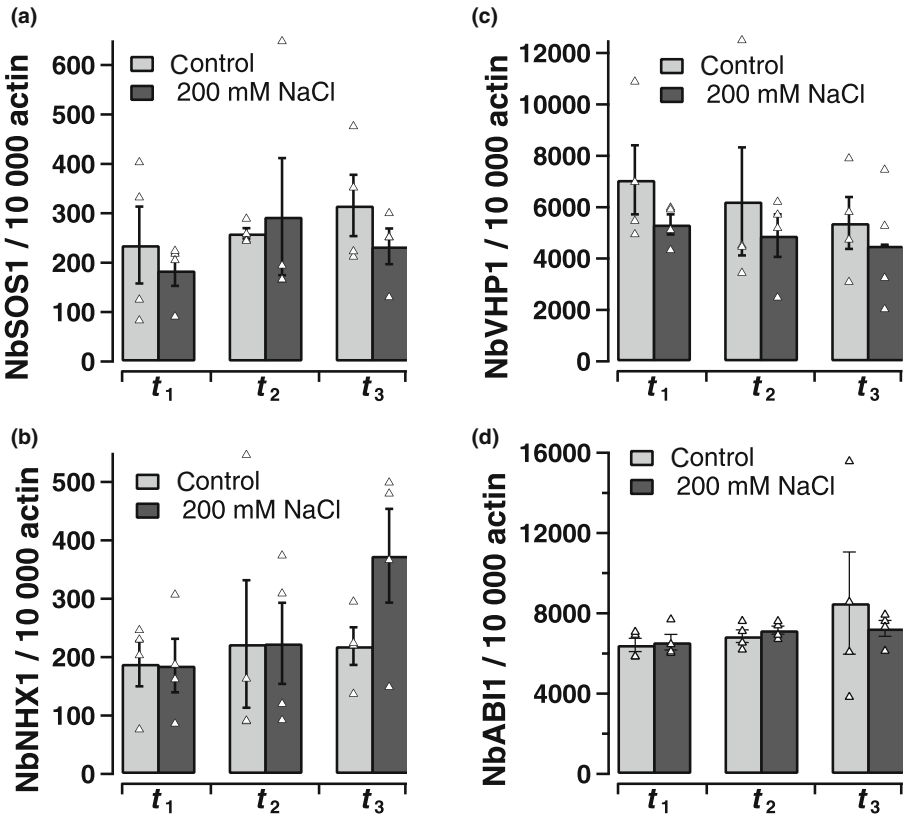

Fig. 4 Transcript level of genes related to salt and osmotic stress in salt-loaded *Nicotiana benthamiana* leaves. Number of transcripts in the leaves loaded with control solution (gray) or with 200 mM sodium chloride (NaCl)-containing solution (black) at time points t_1, t_2 and t_3. Time point t_1 is immediately after infiltration, t_2 is at maximum leaf wilting and t_3 is the time point the leaves recovered from wilting. Transcript numbers of the (a) NbSOS1, (b) NbNHX1, (c) NbVHP1, and (d) NbABI1 genes were normalized to 10 000 actin transcripts. Data points are given as means ± SE ($n = 4$–5), the triangles are individual data points from biological replicates. No significant differences in transcript levels between control and salt-treated leaves was found with two-way ANOVA followed by Tukey's *post hoc* test.

across the plasma membrane of plant cells (Newman, 2001; Böhm *et al.*, 2016; Huang *et al.*, 2021). To expose mesophyll cells to a 200 mM NaCl salt load, we peeled off the lower epidermis. Replacing the bath solution with 200 mM NaCl resulted in a measured H^+ release in response to the NaCl load (Fig. 5b). This effect could be explained by depolarization-dependent activation of AHA2 type H^+-pumps (Cuin & Shabala, 2005; Reyer *et al.*, 2020). In addition to changes in H^+ pump activity, the application of K^+ electrodes in tandem revealed that K^+ fluxes also respond to salt: the K^+ influx vanished, turned direction, and developed into peak outward K^+ fluxes of up to 50 nmol m^{-2} s^{-1} within *c.* 20 min (Fig. 5b; Shabala, 2000). This phenomenon is in line with voltage-dependent GORK-type K^+ efflux channels activating upon salt-induced depolarization (Ache *et al.*, 2000; Reyer *et al.*, 2020).

To study whether Ca^{2+} signals in the mesophyll are involved in leaf responses to salt loads, $[Ca^{2+}]_{cyt}$ dynamics were monitored in leaf discs of *N. benthamiana* plants expressing the single-wavelength Ca^{2+}-sensor GCaMP3 (DeFalco *et al.*, 2017). In contrast to the common view that salt triggers Ca^{2+} rises (Köster *et al.*, 2019), no Ca^{2+} signals were set off in the mesophyll upon 200 mM NaCl treatment (Fig. 5c,d). In line with the Ca^{2+} measurements in guard cells (Fig. 2b–d), only a pronounced $[Ca^{2+}]_{cyt}$ increase was monitored in the mesophyll upon NaCl removal and returning to the salt-free control solution (Fig. 5c,d). Remarkably, this $[Ca^{2+}]_{cyt}$ increase spread through the tissue as a $[Ca^{2+}]_{cyt}$ wave (Video S2; Fig. 5c,d). Despite the lack of symplastic connectivity between guard- and mesophyll cells (Wille & Lucas, 1984), transient elevations in $[Ca^{2+}]_{cyt}$ were detected in guard cells (arrows in Fig. 5c) when the mesophyll $[Ca^{2+}]_{cyt}$ wave passed by them (Video S2).

Although there is ample evidence that salt stress leads to $[Ca^{2+}]_{cyt}$ signals, we did not observe them in guard cells (Fig. 2) or in the mesophyll at the cellular and tissue levels (Fig. 5). To transfer these results from the cellular level to the macroscopic level, and to verify whether the turgor-loss-recovery cycle upon salt infiltration in the intact leaves requires Ca^{2+} signals, we again monitored salt induced leaf movements. The infiltrated salt solution now contained the Ca^{2+} channel blocker lanthanum ($LaCl_3$), that has already been reported to effectively block NaCl-induced Ca^{2+} signals (Choi *et al.*, 2014). In the absence or the presence of lanthanum, the turgor-loss-recovery cycle of leaves had the same magnitude (Fig. S7a,b) and timing (Fig. S7c), which strongly indicated that Ca^{2+}-signaling is not required for salt redistribution in intact tobacco leaves.

Salt responses require vacuolar NHX1 independent from regulation via cytosolic Ca^{2+}

To test for the interconnection between membrane energization and cytosolic pH and/or Ca^{2+} control in the salt stress response of the intact leaf tissue, we monitored the membrane potential simultaneously with $[Ca^{2+}]_{cyt}$ and $[H^+]_{cyt}$ using the dual Ca^{2+}/H^+-sensor CapHensor in *N. benthamiana* leaf discs (Li *et al.*, 2021; Figs 6, S8). For stable electrode-based membrane voltage recordings, mesophyll cells were challenged with 50 mM rather than 200 mM NaCl to avoid turgor loss (Shahzad *et al.*, 2013; Isayenkov & Maathuis, 2019). Therefore, the salt

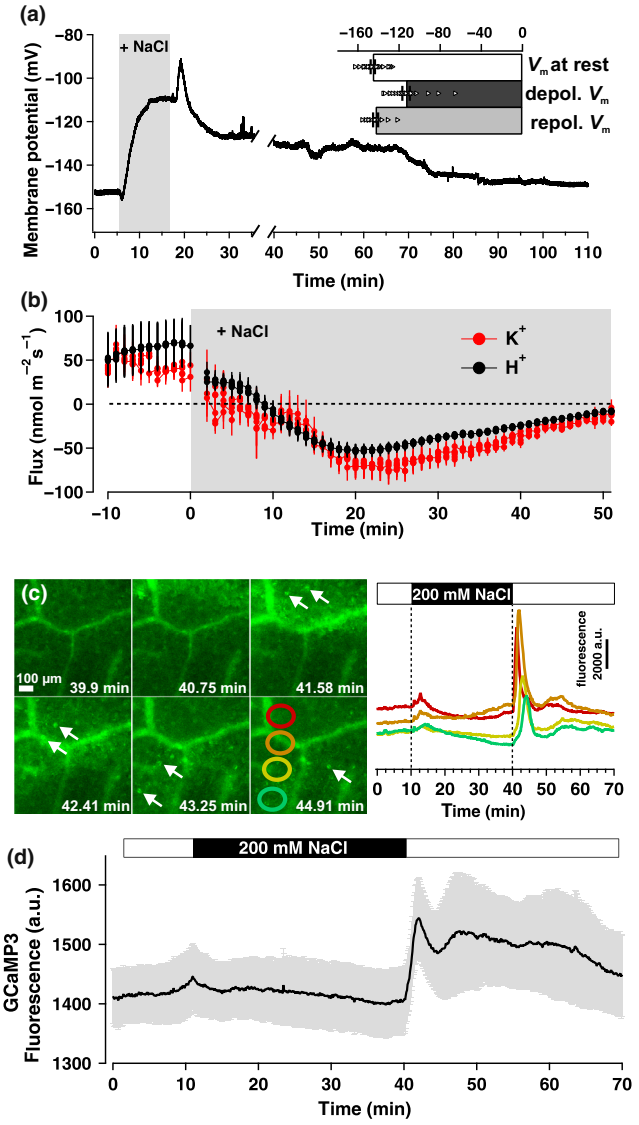

Fig. 5 Salt-induced change in membrane voltage, ion fluxes and calcium ion (Ca^{2+})-dynamics in *Nicotiana benthamiana* mesophyll cells. (a) The free-running membrane potential (V_m) from mesophyll cells at the rim of a leaf disc in the absence and presence of high salt loads (200 mM sodium chloride (NaCl), gray bar) in the bath medium. The inlay in (a) displays V_m at rest before salt perfusion (white bar), at steady-state depolarization (black bar) in the presence of salt, and at the subsequent repolarized V_m (gray bar). Data in bar diagram represents means ± SE ($n = 10$) and triangles are the individual measurements from different leaves. (b) Recording of extracellular potassium ion (K^+) and hydrogen ion (H^+) fluxes from mesophyll cells by means of ion-selective electrodes in response to 200 mM NaCl (as indicated by the gray area). Positive and negative fluxes correspond to import or release of the respective cation, respectively. Data points are given as means ± SE (each $n = 11$). (c, d) Cytosolic Ca^{2+} recording in a stable expressing GCaMP3 *N. benthamiana* leaf disc. (c) False-colored fluorescence images of a representative time-lapse series showing a Ca^{2+}-wave moving from top to bottom. The signal-over-time plot (right side) represents the GCaMP3 fluorescence from the colored marked areas (on the left side), showing a time-shift in Ca^{2+} signals from regions top to bottom upon wash-out but not wash-in of 200 mM NaCl. This Ca^{2+}-wave in the mesophyll sets off Ca^{2+}-signals in guard cells (as indicated by arrows, see Video S2). (d) Mean changes (black line) ± SE (gray area) in GCaMP3 fluorescence from the same time-series as shown in (c), when NaCl was applied for 30 min ($n = 6$ independent experiments with different leaf samples).

media and NaCl-free control solutions were osmotically balanced. In contrast to control experiments with perfused NaCl-free solution of constant osmolality throughout the same recording time (Fig. S9), the membrane potential (black line) dropped *c.* 40 mV when 50 mM NaCl was applied ($n = 11$, Fig. 6a,b). At the same time, $[Ca^{2+}]_{cyt}$ (red line) slightly decreased and the pH (green line) alkalized (Figs 6a, S8a). Upon termination of the salt challenge, all three signals showed pronounced transient overshoots before returning to their pre-stimulus levels (Figs 6a, S8a). To change the leaf vacuole Na^+ uptake capacity, we overexpressed the cation/H^+ transporter AtNHX1 together with the CapHensor in *N. benthamiana* leaves. Vacuolar localization of AtNHX1 (and AtNHX2) was reported and confirmed multiple times (Apse *et al.*, 1999; Quintero *et al.*, 2000; Yokoi *et al.*, 2002). Therefore, we stepped back to test subcellular localization of AtNHX1 by fusing it to a fluorescent reporter protein because this would have resulted in spectral overlap with the CapHensor biosensor introduced to image cellular Ca^{2+} and pH changes. When we monitored responses to NaCl (Figs 6c, S8b), the salt-induced depolarization was found to be significantly smaller ($P < 0.01$; Fig. 6d) with AtNHX1 overexpression compared to leaves expressing only CapHensor (Fig. 6b). At the same time, virtually no changes in $[Ca^{2+}]_{cyt}$ and $[H^+]_{cyt}$ occurred in AtNHX1-overexpressed leaves after NaCl treatment (Figs 6c, S8b). Because the mesophyll cells (Figs 5, 6), like the guard cells (Fig. 2), did not show an increase in $[Ca^{2+}]_{cyt}$ when exposed to NaCl, we compared the leaf cell salt response to that of the root. In good agreement with earlier findings (Choi *et al.*, 2014), we observed pronounced $[Ca^{2+}]_{cyt}$ rises in roots upon NaCl application (Fig. S10). This Ca^{2+} response provides unequivocal evidence that the leaf manages salt stress differently to the roots.

Discussion

Housekeeping transport systems suffice for detoxification of high salt loads

The ability to deliver salt directly to roots and study their responses has led to a firm understanding of the cellular processes taking place during salt detoxification in roots. The cuticle barrier does not allow such simple salt application approaches in leaves, so our knowledge of how to process large amounts of salt entering the leaves is incomplete. Monitoring leaf movements after NaCl infiltration by video camera, however, enabled us to resolve and quantify the timing of the underlining salt redistributing transport mechanisms in leaves (Figs 1, S3). The wilting-recovery cycle was nearly the same with 50, 100, and 200 mM NaCl infiltration, except that the response was most pronounced with 200 mM NaCl (Fig. S1). It indicates that the salt transport capacity of leaves is not yet limited at this high apoplastic NaCl concentration. The recovery phase, after reaching the maximum wilting state, only took about 30–40 min (Figs 1, S3). This rapid salt-processing period did rely on salt uptake from the apoplast (Fig. S3) but was not dependent on either a rise in the water stress hormone ABA or production of the compatible osmolyte proline

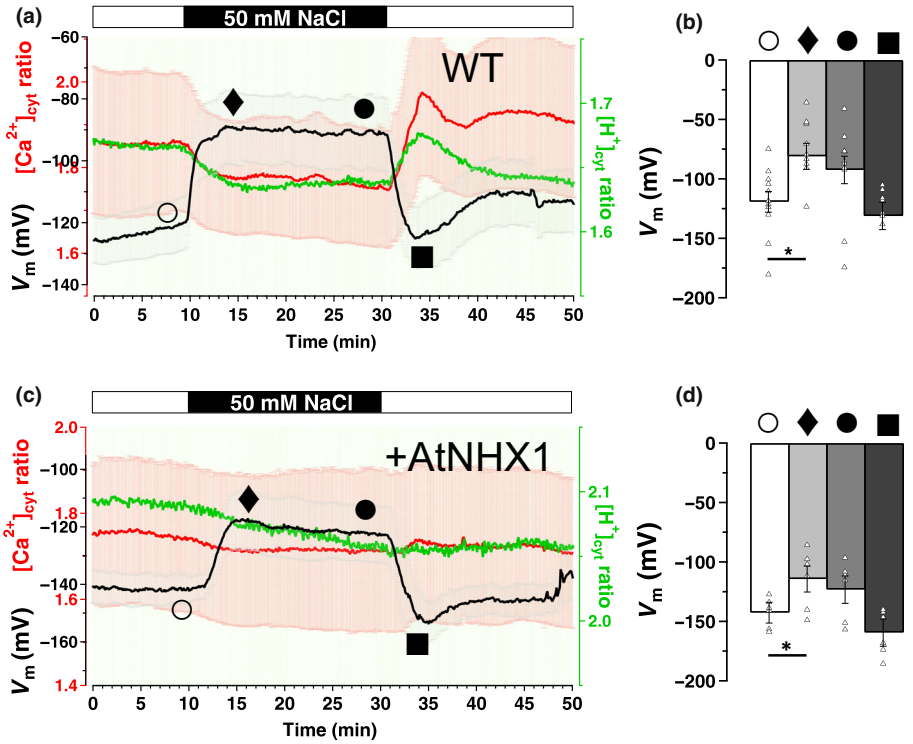

Fig. 6 Vacuolar cation/H^+ antiporter NHX1 dampens salt-induced membrane potential changes and cytosolic calcium ion (Ca^{2+}) and hydrogen ion (H^+) deflections in the mesophyll. (a, c) Sodium chloride (NaCl, 50 mM) treatment during synchronized $[Ca^{2+}]_{cyt}$- and $[H^+]_{cyt}$-ratio imaging and microelectrode-based membrane voltage recordings in *Nicotiana benthamiana* leaf discs. Leaves transiently expressing the dual-reporter CapHensor without (a, $n = 11$) or with (c, $n = 6$) simultaneous expression of AtNHX1. (b, d) Bar diagrams of the mean membrane potential values ± SE before (○), immediately after (◆), at the end of the salt treatment (●) or after washout (■) of 50 mM NaCl from wild-type (WT) leaves (b, $n = 11$) or leaves transiently overexpressing AtNHX1 (d, $n = 6$). Asterisks in (b) and (d) indicate significant differences (*, $P < 0.05$) using unpaired *t*-test between the membrane voltages measured before and immediately after salt exposure. Triangles in (b) and (d) represent individual data points from different biological replicates. The control solution (75 mM MES, 1 mM $CaCl_2$, pH 5.8 adjusted with Tris) was isosmotic to the following solution additionally containing 50 mM NaCl and devoid of a corresponding amount of MES.

(Fig. 3). Instead, Na^+ and Cl^- are taken up into the cytosol and shuttled towards the vacuole salt deposit (Figs 6, S11) which is supported by the finding that high salt loads remain in the very tobacco leaves infiltrated (Graus *et al.*, 2018). The transport of Na^+ and Cl^- as well as the associated membrane potential and pH responses to salt stress onset and termination were immediate (Figs 2, 5, 6, S4, S6). This is consistent with the model that ion transporter networks are capable to rapidly translate the information about changing external solute concentrations into $[H^+]_{cyt}$ and $[Ca^{2+}]_{cyt}$ signals (Dreyer *et al.*, 2022). Interestingly, the function of the cation and anion transport systems in leaves for ion redistribution was not dependent on a rise in $[Ca^{2+}]_{cyt}$ for the regulation of their transcription or transport activity (Figs 2–6, S4, S7, S8), whereas roots of various species are well known to upregulate SOS1 transcripts upon salt treatment (Lekshmy *et al.*, 2015; Darko *et al.*, 2017; Ghorbani *et al.*, 2019). In line with the literature (Behera *et al.*, 2015; Corso *et al.*, 2018; Jeon *et al.*, 2019), we only observed pronounced $[Ca^{2+}]_{cyt}$ increases upon salt wash-out (Figs 2, 5, 6). This behavior may be explained by plasma membrane tension activating mechanosensitive channels permeable for Ca^{2+} in the process of turgor regain and cell swelling (Jiang *et al.*, 2019). These findings indicate that (1) leaf cells, even in their resting state, are already equipped with the relevant transporter systems required for NaCl detoxification (Figs 4, S5), and (2) initial Ca^{2+}-dependent post-translational mechanisms are not required for salt redistribution (Figs 2, 5, 6, S7).

Leaves detoxify sodium by vacuole intake rather than plasma membrane export

In roots, SOS1 is thought to play a major role in ameliorating salt stress, by limiting Na^+ entry (Seifikalhor *et al.*, 2019), whereas the need for vacuolar sequestration of Na^+ in roots seems to apply only in some species (Wu *et al.*, 2019). In contrast, salt tolerance in leaves relies mostly on Na^+ sequestration into vacuoles (Sun *et al.*, 2019). Thus, upon prolonged salt stress Na^+/K^+-ratios in leaves are higher than in roots (Dong *et al.*, 2015; Baetz *et al.*, 2016; Darko *et al.*, 2017; Graus *et al.*, 2018). Although the Na^+ and K^+ cation import transporters are genetically identified as members of HKT1-type Na^+ channels (Böhm *et al.*, 2018; Riedelsberger *et al.*, 2021), AKT1 Shaker-type K^+_{in} channels and proton-driven high-affinity K^+-transporters (HAK5; Véry *et al.*, 2014; Scherzer *et al.*, 2015), the molecular identity of the plasma membrane anion uptake transporter(s) remains to be identified (Geilfus, 2018). In response to salt stress, the plasma

membrane of both root and leaf cells depolarize (Figs 5, 6, S6; Cuin *et al.*, 2008), but in plants overexpressing AtNHX1, we found that NaCl-dependent depolarization was largely suppressed (Fig. 6). From live-cell experiments with the CapHensor (Li *et al.*, 2021), we found that the enhanced shuttling of Na^+ into the vacuole via increased number of NHX1 transporters does not only feedback on the plasma membrane potential of leaf cells. It also suppresses cytosolic alkalization (Figs 6, S11). So far, we can only speculate about the vacuole-plasma membrane signaling and pH-dependent regulation from the NHX1 luminal side (Yamaguchi *et al.*, 2005). Nevertheless, our results are in line with Gradogna *et al.* (2021) suggesting that NHX1 causes cytosolic acidification/vacuolar alkalization through its Na^+/H^+ antiport mechanism when high salt concentrations are present in the cytosol. Thus, enhanced shuttling of Na^+ into the vacuole when overexpressing NHX1 in mesophyll likely counteracts the salt-dependent alkalization of the cytosol (Figs 6, S11).

Conclusion

The current opinion of salt stress tolerance is that the root is the major player in both salt excluder and includer plants. The root is seen as a 'firewall' for Na^+ and Cl^- entry into the shoot, which is assumed unable to tolerate higher salt doses. In contrast to knowledge mostly gained with seedlings (Cao *et al.*, 2017; Jiang *et al.*, 2019) or roots (Choi *et al.*, 2014; Feng *et al.*, 2018), our studies with tobacco document that mature leaves already have the house-keeping transporter inventory to cope with sudden strong salt loads in the apoplast, even with levels as high as 200 mM. This shows that plants can respond rapidly to even severe changes in their environment without changes in gene expression (Figs 4, S5).

In contrast to root cells, which show $[Ca^{2+}]_{cyt}$ signals and cytosolic alkalization after salt stress (Fig. S10), no $[Ca^{2+}]_{cyt}$ signals are generated in tobacco leaves (Figs 2, 5, 6), indicating an organ-specific processing of salt stress.

Acknowledgements

The work was funded by the Deutsche Forschungsgemeinschaft to KRK (DFG KO3657/2-3), RH (DFG SCHE2148/1-1) and by a doctoral fellowship from the China Scholarship Council to KL and MD. The authors thank Rob Roelfsema for critical reading of the manuscript. The authors also thank Masatsugu Toyota and Simon Gilroy for providing transgene 35S::GCaMP3 expressing *N. benthamiana* seeds. Open Access funding enabled and organized by Projekt DEAL.

Competing interests

None declared.

Author contributions

KRK, IM and RH designed the research. KL, DG, JMR, MD, MK and SS performed research and KL, DG, JMR, MD, MK and SS analyzed data. KL, DG, MD, MK, MJM, SS, TAC, KASA-R, IM and KRK interpreted data. KRK, IM and RH wrote the article. KL and DG contributed equally to this work.

ORCID

Khaled A. S. Al-Rasheid https://orcid.org/0000-0002-3404-3397
Meiqi Ding https://orcid.org/0000-0001-5035-6062
Dorothea Graus https://orcid.org/0000-0001-9709-3941
Rainer Hedrich https://orcid.org/0000-0003-3224-1362
Kai R. Konrad https://orcid.org/0000-0003-4626-5429
Markus Krischke https://orcid.org/0000-0002-2738-0053
Kunkun Li https://orcid.org/0000-0003-1597-197X
Martin J. Müller https://orcid.org/0000-0001-8122-5460
Irene Marten https://orcid.org/0000-0001-8402-869X
Jan M. Rathje https://orcid.org/0000-0003-2927-2870
Sönke Scherzer https://orcid.org/0000-0002-7197-2101

Data availability

The data and materials of this study are available from the corresponding author upon reasonable request.

References

Ache P, Becker D, Ivashikina N, Dietrich P, Roelfsema MR, Hedrich R. 2000. GORK, a delayed outward rectifier expressed in guard cells of *Arabidopsis thaliana*, is a K^+-selective, K^+-sensing ion channel. *FEBS Letters* **486**: 93–98.

Apse MP, Aharon GS, Snedden WA, Blumwald E. 1999. Salt tolerance conferred by overexpression of a vacuolar Na^+/H^+ antiport in *Arabidopsis*. *Science* **285**: 1256–1258.

Arif I, Newman IA, Keenlyside N. 1995. Proton flux measurements from tissues in buffered solution. *Plant Cell and Environment* **18**: 1319–1324.

Assaha DVM, Ueda A, Saneoka H, Al-Yahyai R, Yaish MW. 2017. The role of Na^+ and K^+ transporters in salt stress adaptation in glycophytes. *Frontiers in Physiology* **8**: 509.

Baetz U, Eisenach C, Tohge T, Martinoia E, De Angeli A. 2016. Vacuolar chloride fluxes impact ion content and distribution during early salinity stress. *Plant Physiology* **172**: 1167–1181.

Behera S, Wang N, Zhang C, Schmitz-Thom I, Strohkamp S, Schültke S, Hashimoto K, Xiong L, Kudla J. 2015. Analyses of Ca^{2+} dynamics using a ubiquitin-10 promoter-driven Yellow Cameleon 3.6 indicator reveal reliable transgene expression and differences in cytoplasmic Ca^{2+} responses in Arabidopsis and rice (*Oryza sativa*) roots. *New Phytologist* **206**: 751–760.

Böhm J, Messerer M, Müller HM, Scholz-Starke J, Gradogna A, Scherzer S, Maierhofer T, Bazihizina N, Zhang H, Stigloher C *et al.* 2018. Understanding the molecular basis of salt sequestration in epidermal bladder cells of *Chenopodium quinoa*. *Current Biology* **28**: 3075–3085.

Böhm J, Scherzer S, Krol E, Kreuzer I, von Meyer K, Lorey C, Mueller Thomas D, Shabala L, Monte I, Solano R *et al.* 2016. The venus flytrap *Dionaea muscipula* counts prey-induced action potentials to induce sodium uptake. *Current Biology* **26**: 286–295.

Britto D, Kronzucker H. 2015. Sodium efflux in plant roots: what do we really know? *Journal of Plant Physiology* **186-187**: 1–12.

Cao X-Q, Jiang Z-H, Yi Y-Y, Yang Y, Ke L-P, Pei Z-M, Zhu S. 2017. Biotic and abiotic stresses activate different Ca^{2+} permeable channels in *Arabidopsis*. *Frontiers in Plant Science* **8**: 83.

Carillo P, Gibon Y. 2011. *PROTOCOL: Determination of glycine betaine. Prometheus Wiki.* [WWW document] URL https://prometheusprotocols.net/function/tissue-chemistry/secondary-compounds/extraction-and-determination-of-glycine-betaine/ [accessed 11 October 2022].

Chen L-Q, Cheung LS, Feng L, Tanner W, Frommer WB. 2015. Transport of sugars. *Annual Review of Biochemistry* **84**: 865–894.

Choi W-G, Toyota M, Kim S-H, Hilleary R, Gilroy S. 2014. Salt stress-induced Ca^{2+} waves are associated with rapid, long-distance root-to-shoot signaling in plants. *Proceedings of the National Academy of Sciences, USA* **111**: 6497–6502.

Conn S, Gilliham M. 2010. Comparative physiology of elemental distributions in plants. *Annals of Botany* **105**: 1081–1102.

Corso M, Doccula FG, de Melo JRF, Costa A, Verbruggen N. 2018. Endoplasmic reticulum-localized CCX2 is required for osmotolerance by regulating ER and cytosolic Ca^{2+} dynamics in *Arabidopsis*. *Proceedings of the National Academy of Sciences, USA* **115**: 3966–3971.

Cuin TA, Betts SA, Chalmandrier R, Shabala S. 2008. A root's ability to retain K^+ correlates with salt tolerance in wheat. *Journal of Experimental Botany* **59**: 2697–2706.

Cuin TA, Shabala S. 2005. Exogenously supplied compatible solutes rapidly ameliorate NaCl-induced potassium efflux from barley roots. *Plant and Cell Physiology* **46**: 1924–1933.

Darko E, Gierczik K, Hudák O, Forgó P, Pál M, Türkösi E, Kovács V, Dulai S, Majláth I, Molnár I *et al.* 2017. Differing metabolic responses to salt stress in wheat-barley addition lines containing different 7H chromosomal fragments. *PLoS ONE* **12**: e0174170.

DeFalco TA, Toyota M, Phan V, Karia P, Moeder W, Gilroy S, Yoshioka K. 2017. Using GCaMP3 to study Ca^{2+} signaling in *Nicotiana* species. *Plant and Cell Physiology* **58**: 1173–1184.

Dinneny JR, Long TA, Wang JY, Jung JW, Mace D, Pointer S, Barron C, Brady SM, Schiefelbein J, Benfey PN. 2008. Cell identity mediates the response of *Arabidopsis* roots to abiotic stress. *Science* **320**: 942–945.

Dong L, Wang Q, Manik SMN, Song Y, Shi S, Su Y, Liu G, Liu H. 2015. *Nicotiana sylvestris* calcineurin B-like protein NsylCBL10 enhances salt tolerance in transgenic *Arabidopsis*. *Plant Cell Reports* **34**: 2053–2063.

Dreyer I, Li K, Riedelsberger J, Hedrich R, Konrad KR, Michard E. 2022. Transporter networks can serve plant cells as nutrient sensors and mimic transceptor-like behavior. *iScience* **25**: 104078.

Feng W, Kita D, Peaucelle A, Cartwright HN, Doan V, Duan Q, Liu M-C, Maman J, Steinhorst L, Schmitz-Thom I *et al.* 2018. The FERONIA receptor kinase maintains cell-wall integrity during salt stress through Ca^{2+} signaling. *Current Biology* **28**: 666–675.

Gaxiola RA, Sanchez CA, Paez-Valencia J, Ayre BG, Elser JJ. 2012. Genetic manipulation of a "vacuolar" H^+-PPase: from salt tolerance to yield enhancement under phosphorus-deficient soils. *Plant Physiology* **159**: 3–11.

Geilfus C-M. 2018. Chloride: from nutrient to toxicant. *Plant and Cell Physiology* **59**: 877–886.

Geng Y, Wu R, Wee CW, Xie F, Wei X, Chan PMY, Tham C, Duan L, Dinneny JR. 2013. A spatio-temporal understanding of growth regulation during the salt stress response in *Arabidopsis*. *Plant Cell* **25**: 2132–2154.

Ghorbani A, Omran VOG, Razavi SM, Pirdashti H, Ranjbar M. 2019. *Piriformospora indica* confers salinity tolerance on tomato (*Lycopersicon esculentum* Mill.) through amelioration of nutrient accumulation, K^+/Na^+ homeostasis and water status. *Plant Cell Reports* **38**: 1151–1163.

Goodin MM, Zaitlin D, Naidu RA, Lommel SA. 2008. *Nicotiana benthamiana*: its history and future as a model for plant-pathogen interactions. *Molecular Plant–Microbe Interactions* **21**: 1015–1026.

Gradogna A, Scholz-Starke J, Pardo JM, Carpaneto A. 2021. Beyond the patch-clamp resolution: functional activity of nonelectrogenic vacuolar NHX proton/potassium antiporters and inhibition by phosphoinositides. *New Phytologist* **229**: 3026–3036.

Graus D, Konrad KR, Bemm F, Patir Nebioglu MG, Lorey C, Duscha K, Güthoff T, Herrmann J, Ferjani A, Cuin TA *et al.* 2018. High V-PPase activity is beneficial under high salt loads, but detrimental without salinity. *New Phytologist* **219**: 1421–1432.

Guo Q, Tian XX, Mao PC, Meng L. 2020. Overexpression of *Iris lactea* tonoplast Na^+/H^+ antiporter gene IlNHX confers improved salt tolerance in tobacco. *Biologia Plantarum* **64**: 50–57.

Gutermuth T, Herbell S, Lassig R, Brosche M, Romeis T, Feijo JA, Hedrich R, Konrad KR. 2018. Tip-localized Ca^{2+}-permeable channels control pollen tube growth via kinase-dependent R- and S-type anion channel regulation. *New Phytologist* **218**: 1089–1105.

Gutermuth T, Lassig R, Portes M-T, Maierhofer T, Romeis T, Borst J-W, Hedrich R, Feijó JA, Konrad KR. 2013. Pollen tube growth regulation by free anions depends on the interaction between the anion channel SLAH3 and calcium-dependent protein kinases CPK2 and CPK20. *Plant Cell* **25**: 4525–4543.

Halfter U, Ishitani M, Zhu J-K. 2000. The *Arabidopsis* SOS2 protein kinase physically interacts with and is activated by the calcium-binding protein SOS3. *Proceedings of the National Academy of Sciences, USA* **97**: 3735–3740.

Hedrich R. 2012. Ion channels in plants. *Physiological Reviews* **92**: 1777–1811.

Hedrich R, Sauer N, Neuhaus HE. 2015. Sugar transport across the plant vacuolar membrane: nature and regulation of carrier proteins. *Current Opinion in Plant Biology* **25**: 63–70.

Huang S, Ding M, Roelfsema MRob G, Dreyer I, Scherzer S, Al-Rasheid KAS, Gao S, Nagel G, Hedrich R, Konrad KR. 2021. Optogenetic control of the guard cell membrane potential and stomatal movement by the light-gated anion channel *Gt*ACR1. *Science Advances* **7**: eabg4619.

Isayenkov SV, Maathuis FJM. 2019. Plant salinity stress: many unanswered questions remain. *Frontiers in Plant Science* **10**: 80.

James RA, Munns R, von Caemmerer S, Trejo C, Miller C, Condon TA. 2006. Photosynthetic capacity is related to the cellular and subcellular partitioning of Na^+, K^+ and Cl^- in salt-affected barley and durum wheat. *Plant, Cell & Environment* **29**: 2185–2197.

Jegadeeson V, Kumari K, Pulipati S, Parida A, Venkataraman G. 2019. Expression of wild rice *Porteresia coarctata* PcNHX1 antiporter gene (PcNHX1) in tobacco controlled by PcNHX1 promoter (PcNHX1p) confers Na^+-specific hypocotyl elongation and stem-specific Na^+ accumulation in transgenic tobacco. *Plant Physiology and Biochemistry* **139**: 161–170.

Jeon BW, Acharya BR, Assmann SM. 2019. The Arabidopsis heterotrimeric G-protein β subunit, AGB1, is required for guard cell calcium sensing and calcium-induced calcium release. *The Plant Journal* **99**: 231–244.

Ji H, Pardo JM, Batelli G, Van Oosten MJ, Bressan RA, Li X. 2013. The salt overly sensitive (SOS) pathway: established and emerging roles. *Molecular Plant* **6**: 275–286.

Jiang Z, Zhou X, Tao M, Yuan F, Liu L, Wu F, Wu X, Xiang Y, Niu Y, Liu F *et al.* 2019. Plant cell-surface GIPC sphingolipids sense salt to trigger Ca^{2+} influx. *Nature* **572**: 341–346.

Julkowska MM, Testerink C. 2015. Tuning plant signaling and growth to survive salt. *Trends in Plant Science* **20**: 586–594.

Jung B, Ludewig F, Schulz A, Meißner G, Wöstefeld N, Flügge U-I, Pommerrenig B, Wirsching P, Sauer N, Koch W *et al.* 2015. Identification of the transporter responsible for sucrose accumulation in sugar beet taproots. *Nature Plants* **1**: 14001.

Karimi SM, Freund M, Wager BM, Knoblauch M, Fromm J, Mueller HM, Ache P, Krischke M, Mueller MJ, Müller T *et al.* 2021. Under salt stress guard cells rewire ion transport and abscisic acid signaling. *New Phytologist* **231**: 1040–1055.

Khan MS, Ahmad D, Khan MA. 2015. Trends in genetic engineering of plants with Na^+/H^+ antiporters for salt stress tolerance. *Biotechnology & Biotechnological Equipment* **29**: 815–825.

Köster P, Wallrad L, Edel KH, Faisal M, Alatar AA, Kudla J. 2019. The battle of two ions: Ca^{2+} signalling against Na^+ stress. *Plant Biology* **21**: 39–48.

Kramer DM, Johnson G, Kiirats O, Edwards GE. 2004. New fluorescence parameters for the determination of QA redox state and excitation energy fluxes. *Photosynthesis Research* **79**: 209–218.

Kreps JA, Wu Y, Chang H-S, Zhu T, Wang X, Harper JF. 2002. Transcriptome changes for Arabidopsis in response to salt, osmotic, and cold stress. *Plant Physiology* **130**: 2129–2141.

Kronzucker HJ, Coskun D, Schulze LM, Wong JR, Britto DT. 2013. Sodium as nutrient and toxicant. *Plant and Soil* **369**: 1–23.

Läuchli A, Grattan SR. 2007. Plant growth and development under salinity stress. In: Jenks MA, Hasegawa PM, Jain SM, eds. *Advances in molecular breeding toward drought and salt tolerant crops*. Dordrecht, the Netherlands: Springer, 1–32.

Lekshmy S, Sairam RK, Chinnusamy V, Jha SK. 2015. Differential transcript abundance of salt overly sensitive (SOS) pathway genes is a determinant of salinity stress tolerance of wheat. *Acta Physiologiae Plantarum* **37**: 169.

Li B, Tester M, Gilliham M. 2017. Chloride on the move. *Trends in Plant Science* **22**: 236–248.

Li K, Prada J, Damineli DSC, Liese A, Romeis T, Dandekar T, Feijo JA, Hedrich R, Konrad KR. 2021. An optimized genetically encoded dual reporter for simultaneous ratio imaging of Ca^{2+} and H^+ reveals new insights into ion signaling in plants. *New Phytologist* **230**: 2292–2310.

Liu J, Zhu J-K. 1998. A calcium sensor homolog required for plant salt tolerance. *Science* **280**: 1943–1945.

Małgorzata J, Kabała K. 2015. The role of plasma membrane H^+-ATPase in salinity stress of plants. *Progress in Botany* **76**: 77–92.

Newman IA. 2001. Ion transport in roots: measurement of fluxes using ion-selective microelectrodes to characterize transporter function. *Plant, Cell & Environment* **24**: 1–14.

O'Leary BM, Rico A, McCraw S, Fones HN, Preston GM. 2014. The infiltration-centrifugation technique for extraction of apoplastic fluid from plant leaves using *Phaseolus vulgaris* as an example. *Journal of Visualized Experiments* **19**: 52113.

Palmgren MG. 2001. Plant plasma membrane H^+-ATPases: powerhouses for nutrient uptake. *Annual Review of Plant Physiology and Plant Molecular Biology* **52**: 817–845.

Patel MK, Kumar M, Li W, Luo Y, Burritt DJ, Alkan N, Tran L-SP. 2020. Enhancing salt tolerance of plants: from metabolic reprogramming to exogenous chemical treatments and molecular approaches. *Cell* **9**: 2492.

Qiu Q-S, Guo Y, Dietrich MA, Schumaker KS, Zhu J-K. 2002. Regulation of SOS1, a plasma membrane Na^+/H^+ exchanger in *Arabidopsis thaliana*, by SOS2 and SOS3. *Proceedings of the National Academy of Sciences, USA* **99**: 8436–8441.

Quintero FJ, Blatt MR, Pardo JM. 2000. Functional conservation between yeast and plant endosomal Na^+/H^+ antiporters 1. *FEBS Letters* **471**: 224–228.

Raddatz N, Morales de los Ríos L, Lindahl M, Quintero FJ, Pardo JM. 2020. Coordinated transport of nitrate, potassium, and sodium. *Frontiers in Plant Science* **11**: 247.

Raschke K, Monteith JL, Weatherley PE. 1976. How stomata resolve the dilemma of opposing priorities. *Philosophical Transactions of the Royal Society of London. Series B: Biological Sciences* **273**: 551–560.

Razavizadeh R, Ehsanpour AA, Ahsan N, Komatsu S. 2009. Proteome analysis of tobacco leaves under salt stress. *Peptides* **30**: 1651–1659.

Reyer A, Häßler M, Scherzer S, Huang S, Pedersen JT, Al-Rasheid KAS, Bamberg E, Palmgren M, Dreyer I, Nagel G *et al.* 2020. Channelrhodopsin-mediated optogenetics highlights a central role of depolarization-dependent plant proton pumps. *Proceedings of the National Academy of Sciences, USA* **117**: 20920–20925.

Riedelsberger J, Miller JK, Valdebenito-Maturana B, Pineros MA, Gonzalez W, Dreyer I. 2021. Plant HKT channels: an updated view on structure, function and gene regulation. *International Journal of Molecular Sciences* **22**: 1892.

Scherzer S, Böhm J, Krol E, Shabala L, Kreuzer I, Larisch C, Bemm F, Al-Rasheid KA, Shabala S, Rennenberg H *et al.* 2015. Calcium sensor kinase activates potassium uptake systems in gland cells of venus flytraps. *Proceedings of the National Academy of Sciences, USA* **112**: 7309–7314.

Seifikalhor M, Aliniaeifard S, Shomali A, Azad N, Hassani B, Lastochkina O, Li T. 2019. Calcium signaling and salt tolerance are diversely entwined in plants. *Plant Signaling & Behavior* **14**: 1665455.

Shabala S. 2000. Ionic and osmotic components of salt stress specifically modulate net ion fluxes from bean leaf mesophyll. *Plant, Cell & Environment* **23**: 825–837.

Shahzad M, Zörb C, Geilfus C-M, Mühling KH. 2013. Apoplastic Na^+ in *Vicia faba* leaves rises after short-term salt stress and is remedied by silicon. *Journal of Agronomy and Crop Science* **199**: 161–170.

Silva P, Gerós H. 2009. Regulation by salt of vacuolar H^+-ATPase and H^+-pyrophosphatase activities and Na^+/H^+ exchange. *Plant Signaling & Behavior* **4**: 718–726.

Stepien P, Johnson GN. 2009. Contrasting responses of photosynthesis to salt stress in the glycophyte *Arabidopsis* and the halophyte *Thellungiella*: role of the plastid terminal oxidase as an alternative electron sink. *Plant Physiology* **149**: 1154–1165.

Stingl N, Krischke M, Fekete A, Mueller MJ. 2013. Analysis of defense signals in *Arabidopsis thaliana* leaves by ultra-performance liquid chromatography/tandem mass spectrometry: jasmonates, salicylic acid, abscisic acid. *Methods in Molecular Biology* **1009**: 103–113.

Subba A, Tomar S, Pareek A, Singla-Pareek SL. 2021. The chloride channels: silently serving the plants. *Physiologia Plantarum* **171**: 688–702.

Sun T-J, Fan L, Yang J, Cao R-Z, Yang C-Y, Zhang J, Wang D-M. 2019. A Glycine max sodium/hydrogen exchanger enhances salt tolerance through maintaining higher Na^+ efflux rate and K^+/Na^+ ratio in Arabidopsis. *BMC Plant Biology* **19**: 469.

Sze H, Chanroj S. 2018. Plant endomembrane dynamics: studies of K^+/H^+ antiporters provide insights on the effects of pH and ion homeostasis. *Plant Physiology* **177**: 875–895.

Véry A-A, Nieves-Cordones M, Daly M, Khan I, Fizames C, Sentenac H. 2014. Molecular biology of K^+ transport across the plant cell membrane: what do we learn from comparison between plant species? *Journal of Plant Physiology* **171**: 748–769.

Voss LJ, Hedrich R, Roelfsema MRG. 2016. Current injection provokes rapid expansion of the guard cell cytosolic volume and triggers Ca^{2+} signals. *Molecular Plant* **9**: 471–480.

Wang H, Ding Q, Wang H. 2018. A new Na^+/H^+ antiporter gene *Kv*NHX1 isolated from the halophyte *Kosteletzkya virginica* improves salt tolerance in transgenic tobacco. *Biotechnology & Biotechnological Equipment* **32**: 1378–1386.

Wang H, Wang H, Shao H, Tang X. 2016. Recent advances in utilizing transcription factors to improve plant abiotic stress tolerance by transgenic technology. *Frontiers in Plant Science* **7**: 67.

Wille AC, Lucas WJ. 1984. Ultrastructural and histochemical studies on guard cells. *Planta* **160**: 129–142.

Wu H. 2018. Plant salt tolerance and Na^+ sensing and transport. *The Crop Journal* **6**: 215–225.

Wu H, Li Z. 2019. The importance of Cl^- exclusion and vacuolar Cl^- sequestration: revisiting the role of Cl^- transport in plant salt tolerance. *Frontiers in Plant Science* **10**: 1418.

Wu H, Shabala L, Zhou M, Su N, Wu Q, Ul-Haq T, Zhu J, Mancuso S, Azzarello E, Shabala S. 2019. Root vacuolar Na^+ sequestration but not exclusion from uptake correlates with barley salt tolerance. *The Plant Journal* **100**: 55–67.

Wu H, Zhang X, Giraldo JP, Shabala S. 2018. It is not all about sodium: revealing tissue specificity and signalling roles of potassium in plant responses to salt stress. *Plant and Soil* **431**: 1–17.

Xiong TC, Ronzier E, Sanchez F, Corratgé-faillie C, Mazars C, Thibaud J-B. 2014. Imaging long distance propagating calcium signals in intact plant leaves with the BRET-based GFP-aequorin reporter. *Frontiers in Plant Science* **5**: 43.

Yamaguchi T, Aharon GS, Sottosanto JB, Blumwald E. 2005. Vacuolar Na^+/H^+ antiporter cation selectivity is regulated by calmodulin from within the vacuole in a Ca^{2+}- and pH-dependent manner. *Proceedings of the National Academy of Sciences, USA* **102**: 16107–16112.

Yang Y, Guo Y. 2018. Unraveling salt stress signaling in plants. *Journal of Integrative Plant Biology* **60**: 796–804.

Yokoi S, Quintero FJ, Cubero B, Ruiz MT, Bressan RA, Hasegawa PM, Pardo JM. 2002. Differential expression and function of *Arabidopsis thaliana* NHX Na^+/H^+ antiporters in the salt stress response. *The Plant Journal* **30**: 529–539.

Yue Y, Zhang M, Zhang J, Duan L, Li Z. 2012. SOS1 gene overexpression increased salt tolerance in transgenic tobacco by maintaining a higher K^+/Na^+ ratio. *Journal of Plant Physiology* **169**: 255–261.

Zhou Y, Ding M, Gao S, Yu-Strzelczyk J, Krischke M, Duan X, Leide J, Riederer M, Mueller MJ, Hedrich R *et al.* 2021a. Optogenetic control of plant growth by a microbial rhodopsin. *Nature Plants* **7**: 144–151.

Zhu J-K. 2002. Salt and drought stress signal transduction in plants. *Annual Review of Plant Biology* **53**: 247–273.

Supporting Information

Additional Supporting Information may be found online in the Supporting Information section at the end of the article.

Fig. S1 The effect of 200, 100, 50 mM NaCl and control solution on the turgor-loss-recovery cycle of *Nicotiana benthamiana* leaves as measured by the droop angle of leaves, time to reach maximum wilting (t_1–t_2) and the time to recover from wilting (t_2–t_3) and (t_1–t_3).

Fig. S2 Recovery from 200 mM NaCl or 200 mM KCl infiltration-induced photosynthetic stress of *Nicotiana benthamiana* leaves measured by the quantum yield of light-induced nonphotochemical fluorescence quenching (Y(NPQ)) at individual times t_1, t_2 and t_3.

Fig. S3 Effect of 200 mM NaCl, 200 mM KCl, 400 mM sucrose and 200 mM sodium gluconate loads on the turgor-loss-recovery cycle of *Nicotiana benthamiana* leaves as measured by the droop angle of leaves at t_2 and t_3, the time to reach maximum wilting (t_1–t_2) and the time to recover from wilting (t_2–t_3) and (t_1–t_3).

Fig. S4 Brightfield and false colored fluorescence $[H^+]_{cyt}$- and $[Ca^{2+}]_{cyt}$-ratio images of *Nicotiana tabacum* guard cells expressing CapHensor upon treatment with 200 mM NaCl and 400 mM mannitol solutions with high osmotic strength or 50 mM NaCl which was iso-osmotic with the control medium.

Fig. S5 Transcript level of genes related to abscisic acid (ABA) and proline synthesis in *Nicotiana benthamiana* leaves at t_1, t_2 and t_3 after infiltration of control medium or 200 mM NaCl solution.

Fig. S6 Salt-induced electric changes of *Nicotiana benthamiana* mesophyll cells and quantification of the membrane voltage before salt treatment and at peak depolarization and repolarization after 200 mM NaCl treatment.

Fig. S7 Quantification of the specific effect of ±1 mM $LaCl_3$ on the wilting-recovery cycle of *Nicotiana benthamiana* leaves upon 200 mM NaCl infiltration as measured by the droop angle of leaves at t_2 and t_3 separately for leaf blades and petioles and through the time required to reach maximum wilting (t_1–t_2) or the time to recover from wilting (t_2–t_3) and (t_1–t_3).

Fig. S8 Brightfield and false colored fluorescence $[H^+]_{cyt}$- and $[Ca^{2+}]_{cyt}$-ratio images of *Nicotiana benthamiana* mesophyll cells expressing CapHensor or co-expressing CapHensor and AtNHX1 upon treatment with 50 mM NaCl.

Fig. S9 Simultaneous recordings of $[Ca^{2+}]_{cyt}$, $[H^+]_{cyt}$ and membrane voltage (V_m) from mesophyll cells of *Nicotiana benthamiana* leaves transiently expressing CapHensor under control conditions.

Fig. S10 Simultaneous $[Ca^{2+}]_{cyt}$ and $[H^+]_{cyt}$ ratio imaging of stably CapHensor expressing *Nicotiana tabacum* roots upon application of 200 mM NaCl.

Fig. S11 Model on salt stress signaling, ion transporter activity and regulation in tobacco leaves for the shuttling of Na^+ into the vacuole for detoxification.

Video S1 Video of leaf and petiole movements with (a) side and (b) front view on *Nicotiana benthamiana* plants infiltrated with salt (200 mM NaCl) solution or control solution.

Video S2 GCaMP3-based detection of salt-induced changes in cytosolic Ca^{2+} of *Nicotiana benthamiana* leaves during perfusion of a 200 mM NaCl loaded solution and wash out 20 min after.

Please note: Wiley Blackwell are not responsible for the content or functionality of any Supporting Information supplied by the authors. Any queries (other than missing material) should be directed to the *New Phytologist* Central Office.